14

4D Printing and Its Biomedical Applications

Saeed Akbari, Yuan-Fang Zhang, Dong Wang, and Qi Ge

Singapore University of Technology and Design, Digital Manufacturing and Design Centre, Singapore 487372, Singapore

14.1 Introduction

In recent years, three-dimensional (3D) printing (also known as additive manufacturing) has emerged as a novel technology to fabricate customized biomedical devices such as stents [1, 2], implants [3, 4], prosthetics [5, 6], and surgical tools [7, 8] with remarkable spatial resolution and design freedom. Moreover, 3D bioprinting was adopted from traditional 3D printing technologies to fabricate biological constructs with the capability of directly encapsulating cells into tissues such as liver, heart, and blood vessels [9–13]. The introduction of 3D printing to the biomedical applications enables the personalization and customization of tissues, drugs, and medical products and devices. Additionally, it is less expensive, and faster than the traditional manufacturing methods, which are commonly used in the biomedical field, and often requires molds, dies, or lithographic masks [14].

However, in many biomedical applications, the dynamic shape changes are desirable but hardly achievable by the conventional 3D printing technologies. For instance, in human and other mammals, the heart has four chambers exhibiting a strong expansion and contraction in each cardiac cycle to pump blood through the blood vessels [15]. Thus, the conventional 3D printing techniques that only create 3D objects with static properties cannot meet the functional requirements of the above-mentioned applications. Dynamic behavior and constantly shape-changing features of biological tissues necessitate the development of a more advanced manufacturing technology.

The recent advances in 4D printing, which adds the fourth dimension "time" to the 3D printed complex structures [16, 17], open a new avenue to 3D printing of biological and medical structures and devices with dynamic behaviors. The 4D printing is realized by creatively integrating engineered active materials into high-resolution 3D printing technologies, which enable the precise deposition of the active materials at micron scales. Under environmental stimuli, e.g. temperature, water, and light [18–21], the properties of the active materials change, which subsequently result in the shape changes of the 3D printed structures over time.

3D and 4D Printing in Biomedical Applications: Process Engineering and Additive Manufacturing,
First Edition. Edited by Mohammed Maniruzzaman.

Despite great progress in the field of 4D printing, its further development for biomedical applications requires the development of novel stimuli-responsive 3D printable biomaterials, advanced 3D printing technologies capable of efficient and rapid deposition of multiple active materials, and computational design tools incorporating realistic material models to predict the 3D printed object behavior under environmental stimuli. This chapter will discuss the potentials of 4D printing as the next-generation technology to fabricate complex 3D biomedical devices and biological structures exhibiting dynamic shape change capability. In this chapter, we will first introduce state-of-the-art 3D printing technologies with potential applications to 4D printing. Then, we will review a number of soft active materials (SAMs) that are widely used in 4D printing. Also, some recent applications of 4D printing in biomedical engineering are presented in detail. At the end, future perspectives of 4D printing in creating novel biomedical devices and bioinspired architectures that can be activated by external stimuli to create highly complex shapes are discussed.

14.2 3D Printing Technologies with Potential for 4D Printing

3D printing or additive manufacturing, which allows the digital design and fabrication of complex 3D objects from various materials with a broad range of mechanical and biological properties, has seen a significant progress over the past three decades [22–24]. Figure 14.1 schematically shows four fundamental categories of 3D printing methods appropriate for effective manufacturing of active structures. These variants of 3D printing offer considerable flexibility in the architecture and properties of structures and will be introduced briefly in this section.

In a conventional 3D printer, a pattern-generating device, typically in the form of a printhead connected to an ink reservoir or a light source, is moved by computer-controlled translation stages. The patterned regions of the printable material are then solidified to produce the desired 3D object. Significant research has been conducted in recent years to increase speed, improve resolution and minimum feature size, and integrate multiple materials into these basic 3D printing technologies [14, 25].

14.2.1 Fused Deposition Modeling (FDM)

In fused deposition modeling (FDM) technology, also known as fused filament fabrication (FFF), a thermoplastic filament is extruded from a nozzle by a worm drive at a controlled rate (Figure 14.2). The nozzle is heated to melt or soften the filament and deposit it on a build tray to fabricate 3D structures in a layer-by-layer manner. The deposited material solidifies after its temperature decreases because of convection heat transfer to the ambient temperature. FDM is the most common 3D printing technology because of its simplicity and low cost. However, compared with other 3D printing technologies, FDM has longer operation time and lower resolution. Moreover, only a few thermoplastic polymers such as acrylonitrile butadiene styrene (ABS) and polylactic acid (PLA) are commercially available for FDM 3D printing.

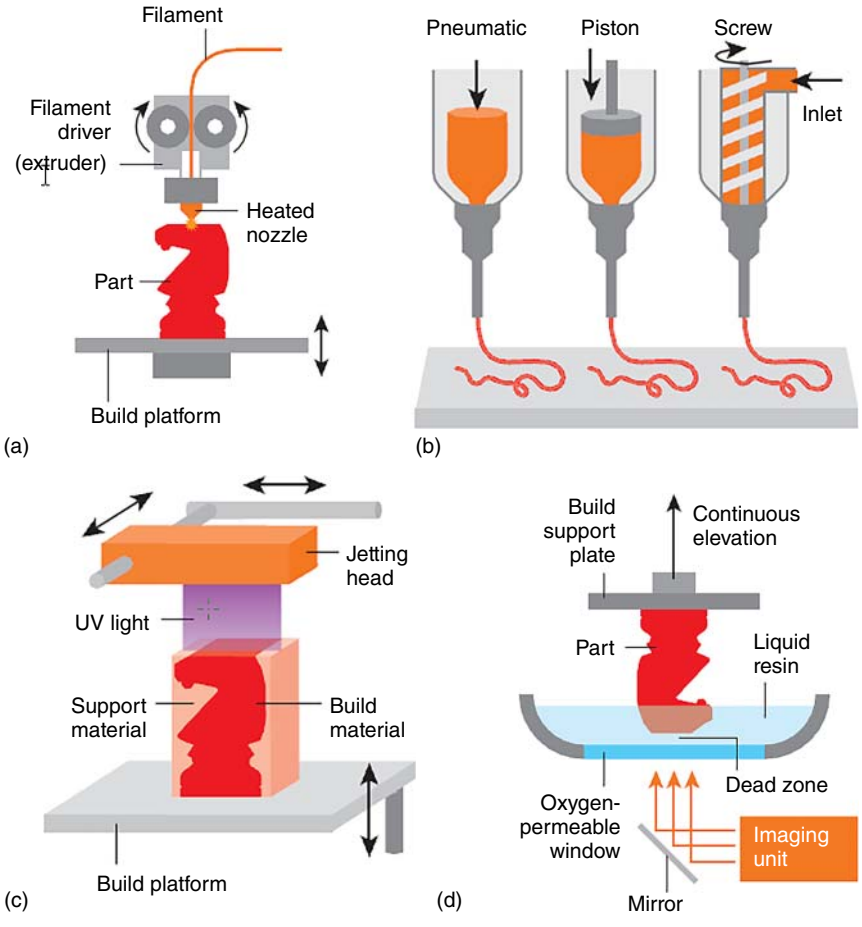

Figure 14.1 Common 3D printing technologies. (a) Fused deposition modeling (FDM), (b) direct ink writing (DIW), (c) inkjet, and (d) projection stereolithography. Source: Truby and Lewis 2016 [14]. Reproduced with permission of Springer Nature.

For specific applications, the initial material should be turned into a filament shape. For example, Yang et al. [26] used a twin-screw extruder to manufacture filaments of a shape memory polymer (SMP) to make it printable using an FDM printer and fabricate a bioinspired robotic finger. Inspired by human finger, each 4D printed finger had three joints printed from the SMP and three rigid segments printed from ABS. Because of the shape memory behavior of the SMP, the finger can be programmed into desired bent shape and then thermally actuated to recover its original shape.

14.2.2 Direct Ink Writing (DIW)

A direct ink writing (DIW) printer uses a printhead similar to an FDM printer. However, instead of a solid thermoplastic, a DIW printer deposits a viscoelastic ink or paste. During printing, the nozzle moves across the build platform and

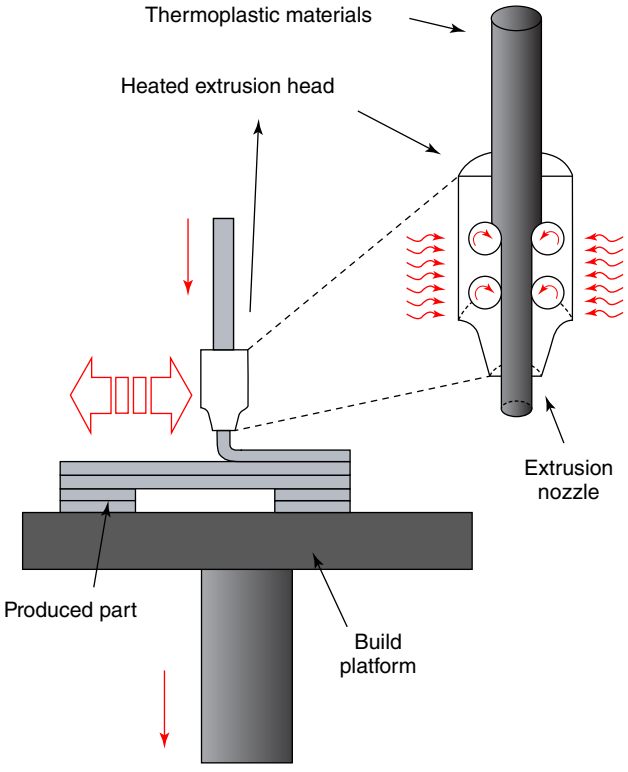

Figure 14.2 Schematics of FDM 3D printing technology. Source: Farahani et al. 2014 [25]. Reproduced with permission of Royal Society of Chemistry.

extrudes the viscoelastic ink under pressure to fabricate the desired 3D object in a layer-by-layer manner. In order to ensure that prohibitively high printing pressures are not required to extrude the viscoelastic ink, it is important to design 3D printable viscoelastic inks that possess significant shear thinning to guarantee efficient extrusion through micro nozzles under ambient conditions. Also, after exiting the nozzle and being deposited on the build tray, the shear thinning materials should have sufficiently high shear elastic modulus and shear yield strength to maintain the desired printed shapes. For this purpose, thickening and thinning agents are typically added to the uncured printing material to modify the respective rheological properties for DIW printing.

Compton and Lewis [27] developed a novel epoxy-based ink to 3D print cellular composites with precise alignment of fiber reinforcement to create hierarchical structures inspired by balsa wood. Although the pure epoxy resin easily flows through the printhead nozzles of a DIW printer, it immediately wets and spreads over the build tray and lacks the ability to support itself. In order to create epoxy inks with desired viscoelastic behavior, nanoclay platelets were used to reinforce the pure epoxy and transform it into a viscoelastic fluid. The resulting epoxy ink exhibited strong shear thinning behavior, with a viscosity of ~20 Pa s at the shear

rate of 50 s^{-1}, which is typical of the DIW printing process, and a viscosity of ~10^4 Pa s at the low shear rate (0.01 s^{-1}). In contrast, the pure epoxy resin has a viscosity of 1.5 Pa s that is independent of shear rate. Consequently, the viscosity of the SiC-filled epoxy is only an order of magnitude higher than that of the pure epoxy under the same printing conditions. In order to effectively design bioinspired hierarchical cellular composites, a computational multiscale model was developed to assess the effect of various design parameters at different levels of microstructural hierarchy on the mechanical properties [28].

Spatial arrangement of multiple ingredients in the printed structure is a grand challenge in 3D bioprinting. Most of the existing DIW bioprinters are limited to the use of a single bioink. Multimaterial DIW bioprinting for the fabrication of sophisticated compositional architectures is often realized by assembling multiple printheads on a single DIW bioprinter [29–31]. This strategy, however, reduces the printing speed as it requires successive switching among the printheads. The switch between nozzles for a typical multinozzle bioprinter on average takes approximately 4–20 seconds [29, 31]. To address this issue, Liu et al. [32] developed a multimaterial DIW bioprinter with a single printhead that is able to continuously pattern multiple bioinks simultaneously. The patterned shear-thinning bioinks were prepared by a suspension of synthetic nanosilicates in water. Multiple bioink reservoirs were routed to a single printhead containing seven bundled channels with equal size and independently actuated by programmable pneumatic valves. Using this technology, different organ-like structures such as brain, heart, liver, kidneys, lung, pancreas, stomach, intestines, bladder, and prostate were printed. This printer exhibits much faster fabrication speed than most available multinozzle printers because it functions continuously without any pause to switch among different materials.

14.2.3 Inkjet

Inkjet is a "noncontact" printing technology that deposits tiny droplets of a low-viscosity ink on a build tray using a thermal or piezoelectric technology. Inkjet printers often combine ink nozzles and a UV light source in one platform. For example, photocurable liquid resins are polymerized immediately after being sprayed on the build tray by illumination with a UV light source (Figure 14.3).

Although accurate placement of cells has been realized through inkjet printing [34], a major limitation of this technology is that it has been designed to deposit low-viscosity inks. Therefore, it is not able to deposit viscous extracellular materials, as the viscosity of the ink in this technology should be less than 0.1 Pa s^{-1}. Small droplet size and low viscosity of the ink have been major obstacles to apply this technology to a broader range of clinical contexts [35].

In order to deposit multiple materials, an inkjet printer can be equipped with multiple printheads, with each printhead spraying a different material (Figure 14.3). This technology, referred to as Polyjet, has been widely used as a versatile technology for 4D printing because it allows for the fabrication of complex three-dimensional solids by micron-scale placement of multiple materials. By controlling the composition of various polymers with highly

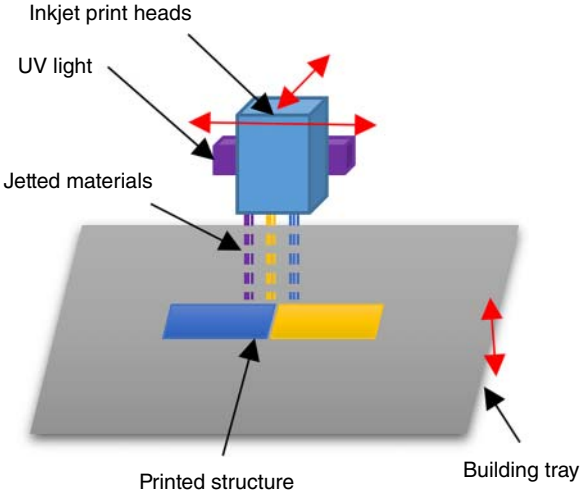

Figure 14.3 Schematics of Polyjet 3D printing technology of liquid photopolymer, which is jetted on a build tray and then UV cured. Source: Adapted from Ding et al. 2017 [33].

different thermomechanical properties as well as changing the spatial variation of constituents over multiple length scales, this technology provides considerable design freedom to produce complex composite structures with controllable anisotropic behavior under thermal and mechanical loadings.

14.2.4 Projection Stereolithography (pSLA)

Stereolithography (SLA), the first 3D printing technology, was developed in 1986 [22]. In this technology, a liquid polymer is selectively polymerized by a rastering laser layer-by-layer to fabricate 3D objects. A major advantage of SLA is that it does not require a nozzle. Thus, the clogging issue commonly observed in other 3D printing technologies could be avoided [36, 37]. However, SLA is relatively slow because it is based on point-source illumination to locally cross-link the polymer.

An alternative method is projection stereolithography (pSLA), also referred to as digital projection lithography (DLP), which is able to polymerize an entire layer using micromirror array devices [38–40]. In pSLA, cross-linking is achieved by projecting a patterned UV light on the surface of a photosensitive polymer resin synergized with upward movement of a linear stage (Figure 14.4). This technology enables the fabrication of complex 3D structures at high resolutions not achievable through the traditional manufacturing technologies. A major limitation of this technology, however, is that it can print only photopolymerizable thermoset resins [14].

In recent years, pSLA has been increasingly used for biofabrication. It allows for precise deposition of biomaterials in relatively small 3D bioconstructs with no adverse effect on cellular viability or functionality [42]. For instance, Ma et al. [41] utilized SLA to print a patient-specific, hydrogel-based model that patterns liver hepatic cells in a physiologically relevant liver-like structure without losing the liver structural and cellular composition (Figure 14.4).

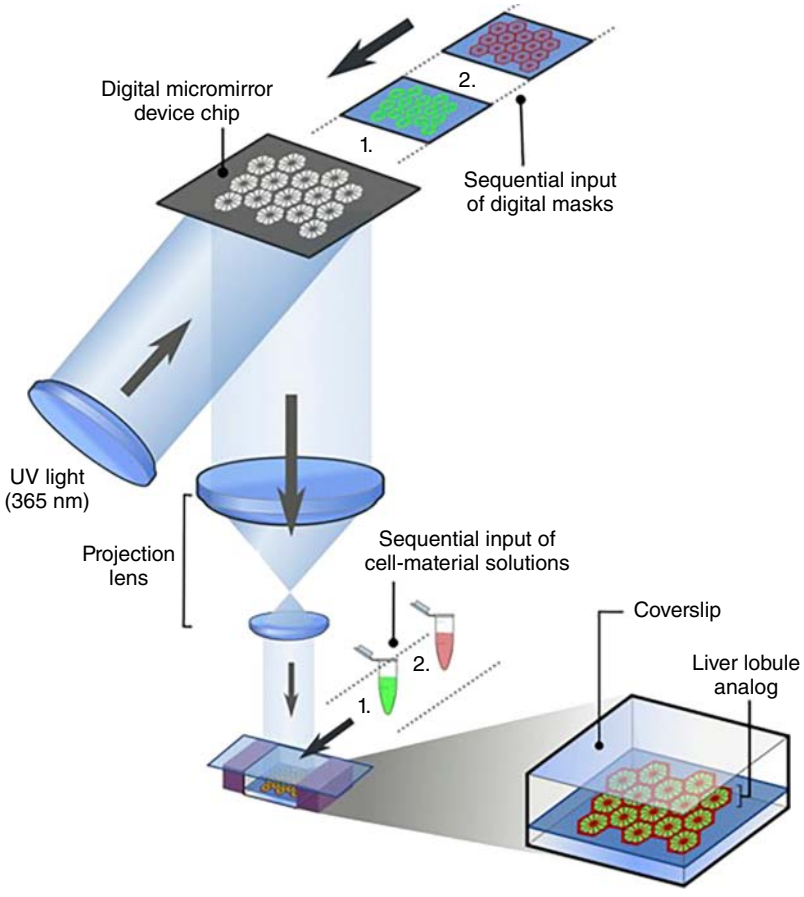

Figure 14.4 pSLA 3D bioprinting of a hydrogel-based hepatic bioconstruct. Source: Ma et al. 2016 [41]. Reproduced with permission of PNAS.

14.3 Soft Active Materials for 4D Printing

The pioneering work advocating the term "4D printing" emerged around 2013 when researchers [16, 17] creatively integrated the SAMs, which exhibit large deformations in response to environmental stimuli, i.e. heat [43, 44], light [45, 46], moisture [47], and others, into 3D printing to create the 3D structures that change shapes over time. Thus, the fourth dimension "time" is added into 3D printing. Despite the rapid development of 4D printing, the most commonly used SAMs for 4D printing are limited to two types: SMPs and hydrogels. In the following, we will introduce these two types of SAMs and the related 4D printing technologies.

14.3.1 Shape Memory Polymers

SMPs are active materials that can recover a predeformed shape under environmental stimuli such as temperature [43, 44, 48–51], light [45, 52–59],

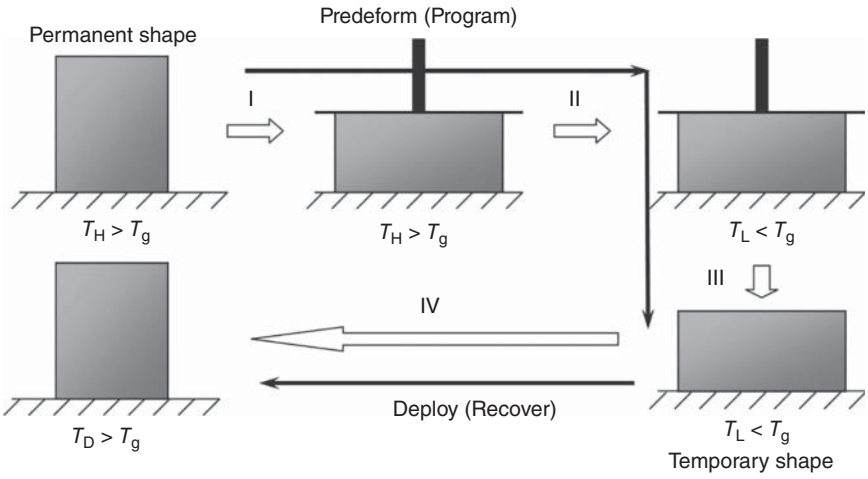

Figure 14.5 A typical thermomechanical loading–unloading cycle in a SMP application. Source: Qi et al. 2008 [67]. Reproduced with permission of Elsevier.

moisture [60], and magnetic field [61]. Compared with the shape memory alloys and ceramics, SMPs possess the advantages of high strain recovery, low density, low cost, easy shape programming procedure, and easy control of recovery. These advantages allow SMPs to be used in many applications such as actuation components in microsystems, biomedical devices, active surface patterning, aerospace deployable structures, and morphing architectures [43, 44, 62–66]. Among the SMPs developed recently, thermally triggered SMPs have been the primary focus in SMP research [65].

For thermally activated SMPs, the most common mechanism used to achieve the shape memory effect is the glass transition that can be obtained following a four-step thermomechanical shape memory cycle (Figure 14.5). At step I, a SMP sample is first deformed at a high temperature T_H ($T_H > T_g$, the phase transition temperature, i.e. glass transition or crystallization temperature) [67]. At step II, the temperature is decreased to a lower one T_L ($T_L < T_g$) while keeping the external constraint. At step III, after removing the external constraint, the SMP sample maintains its deformed shape at T_L. Finally, at step IV, the SMP "remembers" and restores the initial undeformed shape after being heated back to T_H.

The first example of 4D printing with SMPs demonstrated by Ge et al. [16] was printed active composites (PACs) where the prescribed multimaterial microstructures were accurately printed by a multimaterial Polyjet 3D printer (Objet Connex 260, Stratasys, Edina, MN, USA). The base materials loaded onto the printer are a class of elastomers (Tango series) and a class of thermosets (Vero series). A number of digital materials, i.e. composite materials obtained by mixing the two types of base materials at the printing stage, are available with tuned thermomechanical properties ranging from rubbery to glassy at room temperature. Based on the understanding of these thermomechanical behaviors of the SMPs that formed the PACs, a computational design tool was developed to guide the setting of design parameters including geometry, material selection,

material placement, and the programming conditions such as deformation and temperature [68]. By precisely defining the different microarchitectures of the PACs, a simple 3D printed strip sample spontaneously deforms into different configurations including coil, helix, wavy-shaped strips (Figure 14.6a) upon a thermomechanical programming. Following the pioneering work of the PAC by 4D printing, researchers also developed a few other SMP-enabled 4D printing examples realized by the Polyjet 3D printer: (i) active origami by 4D printing where the active hinges were carefully designed to achieve different bending angles at different positions of 2D sheets of airplane. (ii) 4D printed structures with the sequential self-folding realized by intelligently placing active hinges with different glass transition temperatures at different positions to control the order of self-bending [19, 70]. The concept of the sequential self-folding is demonstrated in Figure 14.6b where a mailbox self-assembles from a 2D flat

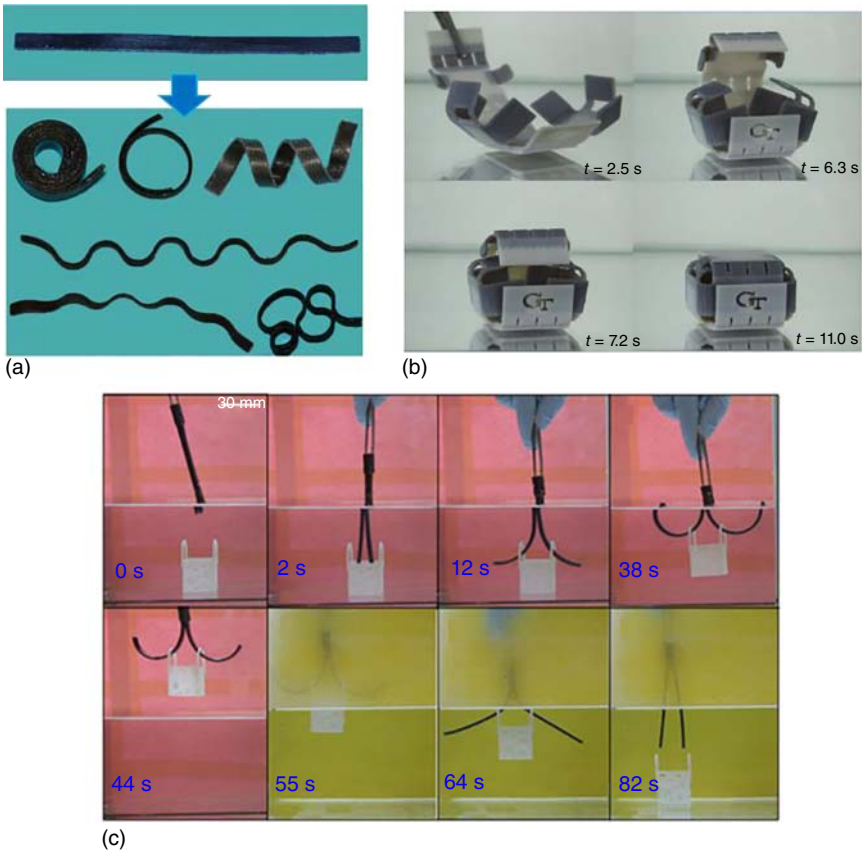

Figure 14.6 (a) A printed strip in its original shape and results of thermomechanical programming with differing fiber architectures. Source: Ge et al. 2013 [16]. Reproduced with permission of AIP. (b) 3D folding structures mimicking the United States Postal Service (USPS) mailbox. Upon heating, the sheet folds into a box with a self-locking mechanism [19]. Source: https://creativecommons.org/licenses/by/4.0/. (c) A smart hook consisting of two SMPs with different T_gs [69]. Source: https://creativecommons.org/licenses/by/4.0/.

sheet into a 3D box with the hinges bending in sequence [19]. (iii) Multishape active composites where SMP fibers with different glass transition temperatures were embedded into an elastomeric matrix to enable a multistep shape memory effect. The recovery of each SMP fiber was triggered only when the ambient temperature exceeded the glass transition temperature [69]. Figure 14.6c demonstrates the multistep recovery in the example of a smart hook that consists of two types of digital SMP fibers embedded in an elastomeric matrix. The glass transition temperatures of the two SMPs are 38 and 57 °C, respectively. The smart hook was first programmed by being stretched by 10%, cooled to 0 °C, and relaxed under 0 °C water for one minute. The first recovery was triggered by placing the smart hook into the warm water with a temperature of 30 °C where the straight strips bend to form two half circular shapes. Using the two half circular strips, a small basket can be lifted from water. To release the box into another position, the temperature of the sample was elevated to be higher than the T_g of all the fibers [69].

Apart from using the commercial Polyjet 3D printer, Ge et al. combined the high-resolution projection microstereolithography (PμSL)-based 3D printing technology with methacrylate-based SMPs to realize high-resolution multimaterial 4D printing [71]. The thermomechanical properties (i.e. glass transition temperature, rubbery modulus, and failure strain) of the SMPs are highly tailorable by choosing different monomers, cross-linkers, and mixing ratios between the monomer and the cross-linker. The methacrylate SMPs exhibit large deformation, which allows the printed structures to accommodate up to 300% large deformation. In addition, the PμSL-based multimaterial 3D printing technology enables the fabrication of 4D printing structures with different SMPs. In Figure 14.7a, a 3D printed Eiffel Tower standing on a Singapore dollar demonstrates the high-resolution 3D printing, and the bending and recovery behaviors of the Eiffel Tower showcase 4D printing with large deformation. Figure 14.7b demonstrates a potential biomedical application, a cardiovascular stent, which was realized by 4D printing with the methacrylate SMPs, and can undergo large local deformation. Figure 14.7c–e demonstrates the examples of 3D printed structures with multiple SMPs: multimaterial grippers that have the potential to function as microgrippers [72] that can grab objects or drug delivery devices [73, 74] that can release objects. Figure 14.7c shows a number of multimaterial grippers with different designs. In Figure 14.7d, an as-printed closed (open) gripper was opened (closed) after programming and the functionality of grabbing (releasing) objects was triggered upon heating. Figure 14.7e shows time-lapsed images of a gripper grabbing an object. The capability of multimaterial fabrication enables the fabrication of the tips of the grippers with the materials different from the SMPs constructing the joints and the design of the stiffness of the tips based on that of the object to realize a safe contact.

Other than UV curing-based SMPs that are thermosets with covalent chemical cross-links, thermoplastic SMPs that are networks with physical cross-links have also been applied to 4D printing. Recently, Yang et al. [21] utilized FDM 3D printing to fabricate 3D structures made of active polymer polyurethane (PU) reinforced with carbon black to introduce the photoresponse. Because of the excellent photothermal conversion efficiency of carbon black ($92 \pm 3\%$) upon illumination,

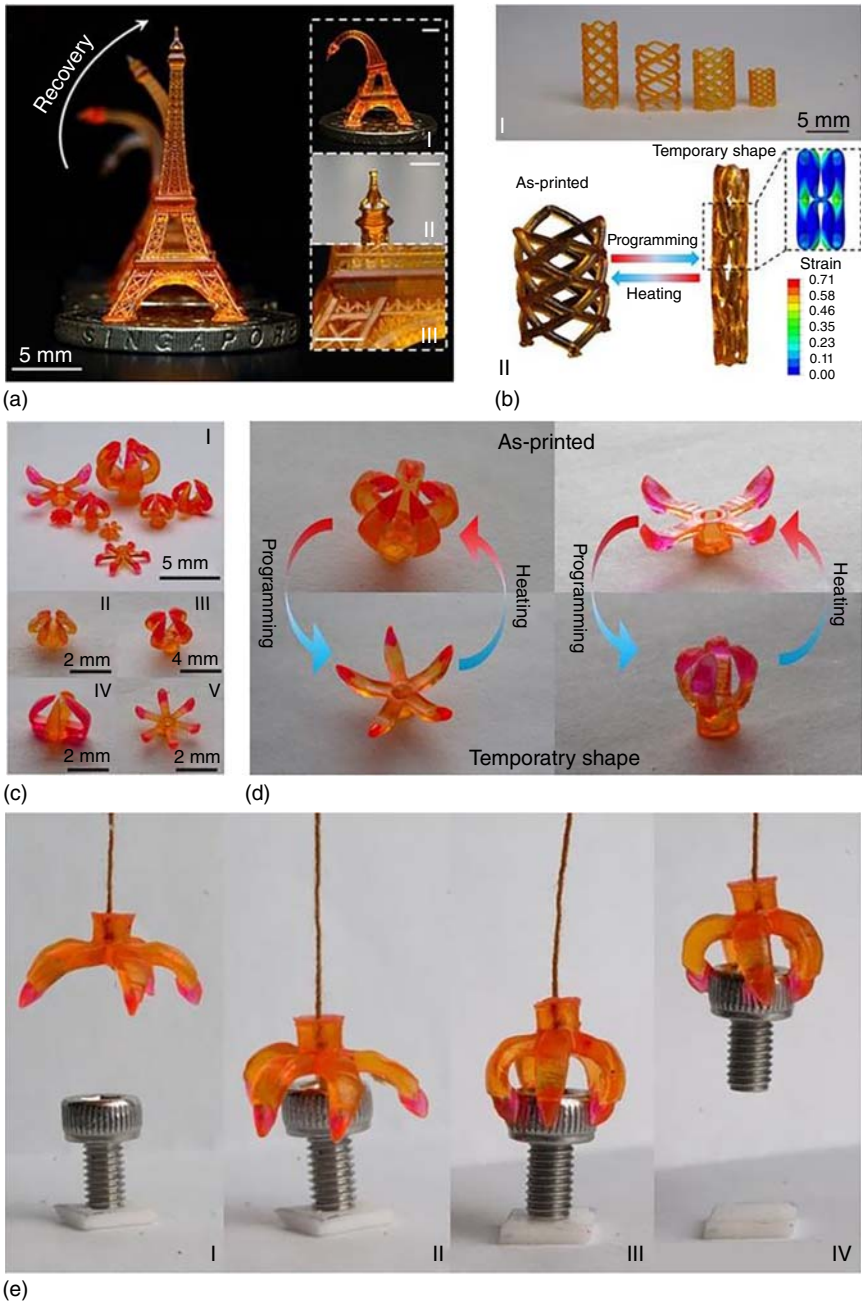

Figure 14.7 (a) 3D printed shape memory (SM) Eiffel Tower. (b) 3D printed SM stents. (c) Multimaterial grippers were fabricated with different designs. (d) Demonstration of the transition between as-printed shape and temporary shape of multimaterial grippers. (e) Snapshots of the process of grabbing an object [71]. Source: https://creativecommons.org/licenses/by/4.0/.

the temperature of the printed structure increases by 20 °C within 10 minutes. The concept of this 4D printing technology was demonstrated via the blooming of a 3D printed sunflower. The petals of the flower gradually opened during illumination under 87 mW cm^{-2} of light intensity, and the temperature increased from 0.4 to 34.4 °C within 280 seconds.

14.3.2 Hydrogels

Hydrogels are another type of SAMs that have been widely applied to 4D printing. They are formed with loosely cross-linked networks of long polymer chains that swell into a larger volume after water or other solvent diffuses into them [75–77]. The essence of designing a 4D printed structure with hydrogels is to design multilayer joints consisting of a layer of elastomer that provides elasticity and a layer of hydrogel that swells in water resulting in the bending of the joint. The first 4D printing example with hydrogels was realized by a Stratasys multimaterial Polyjet 3D printing [17]. It was demonstrated by a straight strand evolved into the "MIT" pattern in the aqueous environment. This self-assembly was realized by precise printing of the hydrogel/elastomer smart hinges. Following this spirit of design, numerous structures exhibiting complex self-evolving deformations were created including sinusoidal waves, hyperbolic surfaces, double-curvature surfaces, time-varying curve (Figure 14.8) [20], etc.

Other than using the Polyjet 3D printing technology, 4D printing with hydrogels can also be realized by employing the DIW 3D printing technology. In Figure 14.9, Gladman et al. [18] developed a bioinspired shape-changing

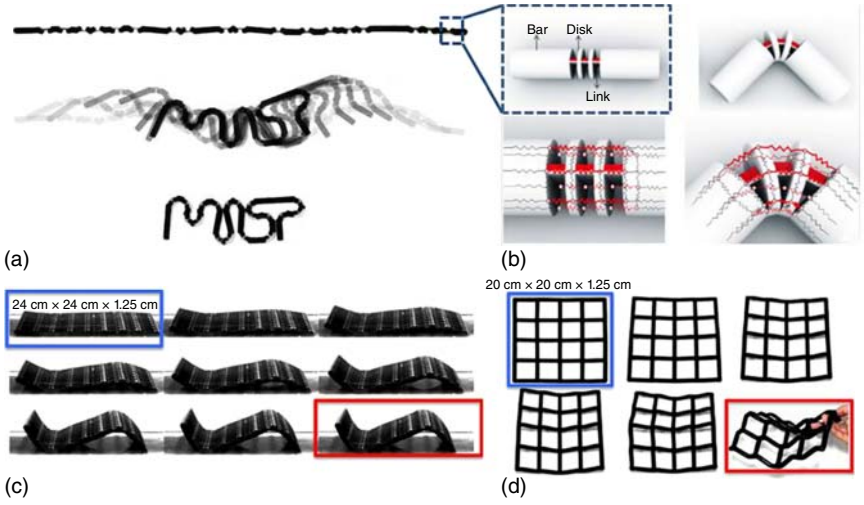

Figure 14.8 Demonstrations of 4D printing presented by the Skyler Tibbits' research group [20]. (a) The self-assembly process from a strand to the "MIT" pattern. (b) The design of a folding joint consisting of a layer of white elastomer providing elasticity and a layer of hydrophilic material that swells after water diffusion and causes the bending of the joint. (c) Deformation of a grid into a sinusoidal wave. (d) Deformation of a grid into a hyperbolic surface [20]. Source: https://creativecommons.org/licenses/by/4.0/.

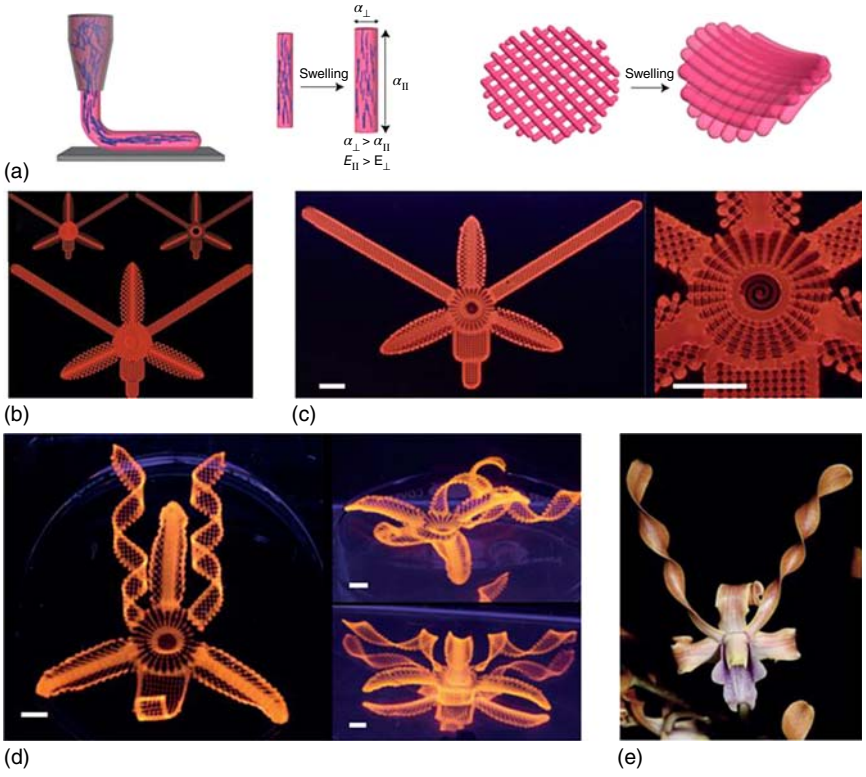

Figure 14.9 Biomimetic 4D printing (Gladman et al.) [18]. (a) Schematic of the shear-induced alignment of cellulose fibrils during direct ink writing and subsequent effects on anisotropic stiffness E and swelling strain α. Print path (b), printed structure (c), and resulting swollen structure (d) of a flower demonstrating a range of morphologies inspired by a native orchid. (e) Based on the print path, this orchid architecture exhibits four different configurations: bending, twisting, and ruffling corolla surrounding the central funnel-like domain (scale bars, 5 mm). Source: Gladman et al. 2016 [18]. Reproduced with permission of Springer Nature.

structure based on 4D printing. Using the DIW technology, they printed a hydrophilic composite material with local control of the orientation of cellulose fibrils within a hydrogel matrix. During printing, fibrils were arranged to induce anisotropic swelling behavior in the longitudinal direction compared to the transverse direction (Figure 14.9a). By following the printing path (Figure 14.9b), generated by a mathematical model that combines thermal expansion in bilayers with a tailored metric-driven approach that employs anisotropic swelling to control the embedding of a complex surface, the printed patterns mimic complex flower morphologies (Figure 14.9c–e) with different configurations.

Another level of actuation can be added to certain hydrophilic materials through the volume change because of the variation of the swelling ratio as a function of temperature [78]. The interpenetrating network of alginate and poly(*N*-isopropylacrylamide) (PNIPAAm) was used for DIW-based 3D printing. PNIPAAm is a thermally responsive hydrogel that was synthesized

from *N*-isopropylacrylamide, a type of commercially available monomer. Upon heating in water above its lower critical solution temperature (LCST) (32–35 °C), PNIPAAm undergoes a coil–globule transition causing a large reversible volume transition. In this process, the material loses its hydrophilicity and hence experiences a large decrease in the water content. A smart valve is created by printing the dynamic hydrogel ink alongside other static materials to control the flow of water in response to the temperature of the water.

14.3.3 Other SAMs

The current 3D printing technologies being costly and time-consuming, some recent advances in 4D printing address these intrinsic drawbacks of 3D printing. For example, a new approach to 4D printing, named direct 4D printing, has recently been proposed by Ding et al. [33] who explored the built-in compressive strain generated during photopolymerization and the mismatch of coefficients of thermal expansion between the elastomer and the SMP in a composite laminate to achieve bending that turns a printed 2D flat sheet into a 3D structure (Figure 14.10a). A structure in its as-printed (temporary) configuration can be deformed to a new shape after removal from the build tray and upon heating that causes the SMP to soften and hence to release the residual strain on the elastomer layer. Cooling down the structure results in a significant increase in the stiffness of the SMP, rendering the new shape permanent. This method makes the fabrication more economical both in terms of time and material consumption compared with the same structure directly printed in three dimensions. The "blooming" of a 4D-printed flower upon heating has been reported elsewhere [33]. The curvatures are merely controlled by varying the layer printing time. A theoretical model is developed to guide the design of structures for direct 4D printing [33, 80]. Ding et al. went further to reduce the dimension of the printed structures to rod elements [79]. Figure 14.10b shows how a 3D buckyball is created by deforming a mesh of 1D rods. This example shows the significant reduction of both printing time (beyond 70%) and material consumption (beyond 90%) that direct 4D printing of rod elements offers in comparison with the same structure printed using conventional 3D printing (Figure 14.10b–d).

Similarly, Huang et al. [81] developed a technique to print thin planar layers with nonuniform cross-linking density distribution by controlling the exposure time at pixel level, requiring, in the meantime, less printing time than the conventional layer-by-layer 3D printing technology. Immersion of the printed structures in water will trigger differential swelling that generates stress causing the structures to deform into 3D objects.

Some other stimulus-response combinations among active materials are less developed for 3D printing, but open interesting perspectives. One example is the 3D printing of pH-responsive polymer to which a postprinting functionalization is applied to form a hydrogel with a tuned degree of swelling [82]. Another example is a computational approach to study the distinct behaviors of thermoresponsive gels and embedded photoresponsive fibers forming a composite in response to heat and illumination [83].

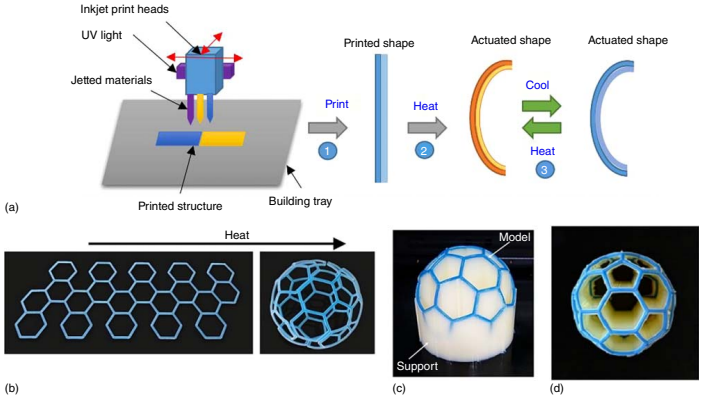

Figure 14.10 (a) The direct 4D printing approach exploits the ability to print controlled multimaterial composites to integrate the five steps into a single one (modified from [33]). (b) A buckyball directly transformed from a planar rod mesh upon heating [79]. The buckyball in conventional 3D printing from (c) isometric view and (d) top view needs to be supported by a large amount of the sacrificial material [79].

14.4 Biomedical Applications of 4D Printing

4D printing has emerged as a versatile technology to fabricate biomedical and bioinspired constructs from active materials. The unique advantage of 4D printing is that it produces structures capable of reshaping under environmental stimuli. For example, oxygen and nutrients are supplied to cells through blood vessels, which are the main channels for vascularization of tissues. Vascularization is a major challenge in fabricating functional tissues. 4D bioprinting is a promising approach to address this issue. Self-folding polymer architectures can be 4D printed to create blood vessels capable of encapsulating blood cells, which subsequently deform into tubelike structures in the presence of water [83]. The following section discusses several examples of the application of 4D printing in biomedical field, with special focus on temperature and humidity-sensitive biostructures.

14.4.1 Temperature-Actuated 4D Printing

The most common external stimulus to actuate the 4D printed structures is temperature. SMPs, including shape memory thermoplastics and shape memory thermosets, are the most commonly used temperature-sensitive active materials in the biomedical field, demonstrate a broad range of mechanical, chemical, and biological properties [81, 84, 85], and have been widely used to fabricate stents [65, 86], scaffolds [87–89], and grippers [90, 91] (Figure 14.11). For biomedical applications, it is important to develop 3D printable materials with activation temperature, e.g. glass transition temperature (T_g) in thermosets or melting temperature (T_m) in thermoplastics, close to physiological temperature.

Compared with shape memory thermoplastics, shape memory thermosets show better shape fixity and recovery, and their thermomechanical properties can be easily tailored to favorable values, but processing shape memory thermoplastics is easier, which makes them more appropriate for some medical applications. Although shape memory thermoset polymers are mostly printed by SLA or inkjet 3D printing methods [16, 20, 68, 71, 93], FDM is the most common technology to print shape memory thermoplastics [94]. For example, Senatov et al. [87] used FDM technology to fabricate a scaffold from PLA with sufficiently high porosity as well as an appropriate pore size necessary for spreading of cells and nutrients throughout the printed structure (Figure 14.11b). The 4D printed structure demonstrated self-fitting effect, resulting from shape memory feature, and has potential to be used for small bone defect replacement. The printing material, PLA, is a biodegradable and bioactive thermoplastic derived from renewable resources. Presently, PLA is one of the world's most consumed biopolymers.

Shape memory behavior of 4D printed structures has the potential to act as a mechanical stimulation bioreactor for cell culture in tissue engineering applications and can be used in various clinical contexts. Active scaffolds can help regenerate tissues, such as cardiovascular tissues, bones, and muscles, that exhibit dynamic mechanical properties. 4D printing enables the customization of the architecture and shape of the active scaffold to ensure that it fits the specific anatomical defect of each patient. This is achieved by combining advanced 3D

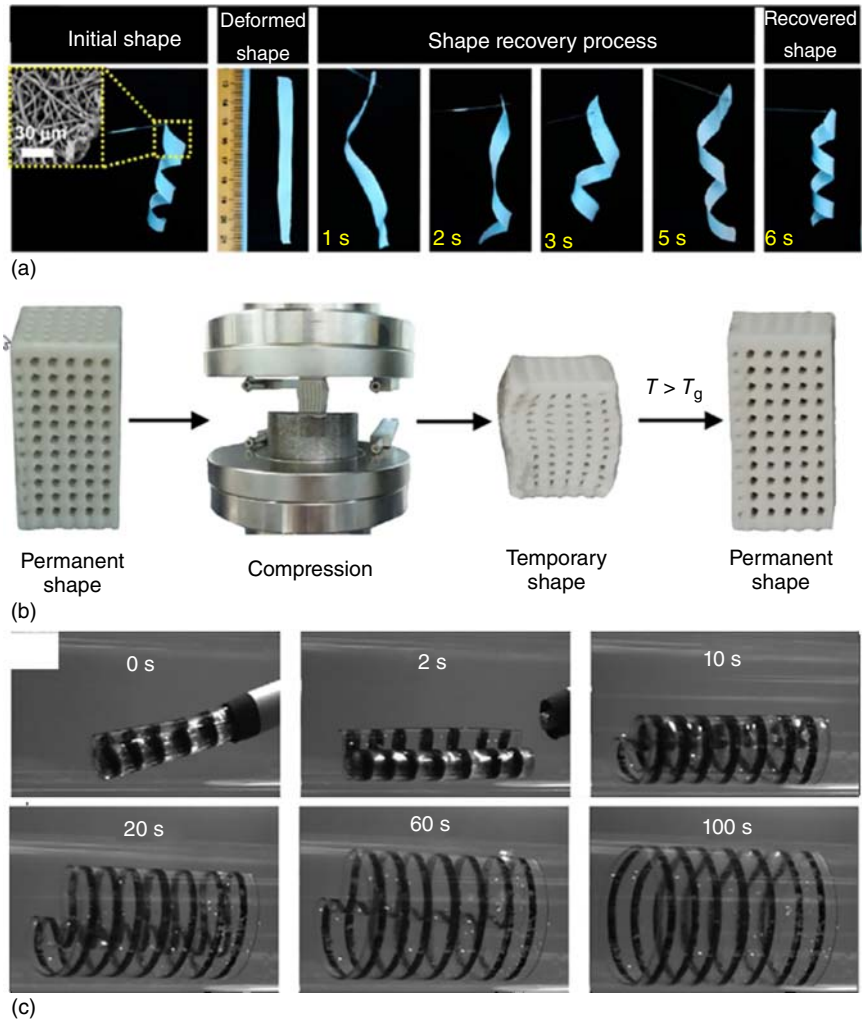

Figure 14.11 Examples of biomedical applications of shape memory polymers. (a) Shape recovery behavior of a poly(D,L-lactide-*co*-trimethylene carbonate) (PLMC) scaffold fabricated by electrospinning. Source: Bao et al. 2014 [92]. Reproduced with permission of ACS. (b) Compression–heating–compression cycles of a PLA-based hydroxyapatite (HA) porous scaffold fabricated by FDM 3D printing technology. Source: Senatov et al. 2016 [87]. Reproduced with permission of Elsevier. (c) Recovery of a cardiovascular stent fabricated from PEGDMA by photopolymerization. Source: Yakacki et al. 2007 [65]. Reproduced with permission of Elsevier.

printing technologies with patient-specific clinical 3D computer-aided design (CAD) images obtained from magnetic resonance imaging (MRI) or computer tomography [95].

Hendrikson et al. [89] used shape memory PU with a T_g of 32 °C to fabricate active scaffolds by FDM technology. The printed scaffolds were loaded at 65 °C using a custom-made stretcher, cooled down to 4 °C, and unloaded to maintain a temporary shape and then seeded by cells cultured at 30 °C to allow for cell

adhesion and proliferation. Finally, the temperature was increased to 37 °C and the permanent shape was recovered. After the shape recovery, cells were significantly more elongated and aligned. In order to facilitate cell activity, the training cycle could be further optimized to apply multiple mechanical stimuli to the cells seeded to the active scaffolds.

One of the potential applications of 4D printing is fabrication of self-deploying stents inserted into lumens, such as coronary artery and trachea, to sustain or keep them open. Zarek et al. [96] designed and printed a smart airway stent using a commercial stereolithography printer. The printed stent is used to sustain the trachea, a flexible, tubular structure that allows for the passage of air from pharynx and larynx to the lungs. It typically has a diameter of 2 cm and a length of approximately 12 cm in adult males.

A common reason for the failure of tracheal stent is migration [97], which can be reduced by customized design approaches based on 3D printing technologies. In order to demonstrate that personalized smart stents can be fabricated with a desired geometry, a digital model of the trachea of a middle-aged male was obtained from an MRI scan. The digital model of the trachea was modified in a CAD software using a Boolean subtraction to convert the model into a shell and to remove the dorsal wall. The stent was then printed from semicrystalline methacrylated polycaprolactone (PCL), a thermoplastic actuated based on the melting temperature (T_m) of the crystalline phase. Terminal methacrylate groups were added to PCL diols to prepare them for stereolithography printing. The printed PCL behaved as a rigid polymer below the T_m and as a flexible elastomer above the T_m. Thermomechanical characterization showed that the T_m of the crystalline phase was 55 °C. However, the T_m of the printed structure can be modified by adjusting PCL molecular weight to achieve desired values of shape fixity and recovery.

The fabricated smart stent was approximately 7 cm long and had a maximum and minimum thickness of almost 3.5 and 1.5 mm, respectively. The thickness of each layer was around 150 μm, and the entire printing process took almost six hours. The shape recovery of the smart stent was demonstrated by heating it in a thermal chamber. The full recovery of the stent was achieved in 14 seconds. After three cycles, a printed stent with a degree of methacrylation of 88% showed a shape fixity of 99% and a shape recovery of 98% [96].

The main source of polymers used to fabricate the biostructures and biomedical devices are conventionally petroleum products. Because these resources are rapidly depleting, the use of plant oils for biopolymer fabrication has attracted significant attention in recent years [98–100]. Plant oil polymers are renewable and exhibit excellent biocompatibility [101]. Miao et al. [93] used a stereolithography apparatus to fabricate smart biocompatible scaffolds from soybean oil epoxidized acrylate, which is a renewable liquid resin for biomedical applications. pSLA has rarely been used to fabricate shape memory scaffolds from liquid resins. Differential scanning calorimetry (DSC) analysis showed that the printed samples had a glass transition temperature (T_g) of 20 °C.

As shown in Figure 14.12, shape memory behavior of the scaffold was examined by bending it into a U shape at human body temperature (37 °C), then fixing the temporary shape by reducing temperature to −18 °C, and finally recovering to its original shape by increasing the temperature to 37 °C. Therefore, the printed

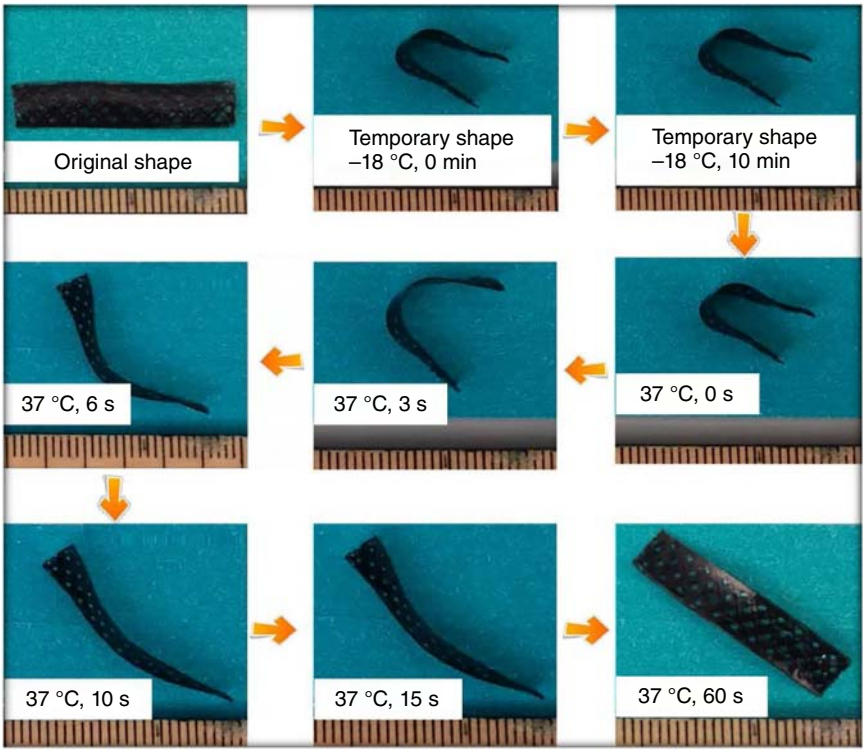

Figure 14.12 Shape memory cycle of the smart scaffold printed from soybean-oil-epoxidized acrylate [93]. Source: https://creativecommons.org/licenses/by/4.0/.

scaffold can be deformed into its temporary shape, embedded in human body, and returned back to its permanent shape with the aid of the body temperature.

Polyethylene glycol diacrylate (PEGDA) resins have been extensively studied to fabricate biomedical scaffolds. However, they are inherently bioinert, and most types of cells are not able to attach to and grow on their surface [102]. Alternatively, PCL and PLA are highly biocompatible polymers, but they lack photosensitive chemical groups and cannot be used for pSLA [103].

In order to evaluate the biocompatibility of the scaffolds printed from soybean oil epoxidized acrylate, Miao et al. studied the attachment of human bone marrow mesenchymal stem cells (hMSCs) on the scaffolds and compared the results with PEGDA, PCL, and PLA [93]. Cytotoxicity analysis indicated that the novel scaffolds printed by stereolithography had better proliferation and adhesion than PEGDA. Moreover, the difference between these new scaffolds, PLA and PCL, was statistically insignificant.

Biomedical devices and natural organs often possess different materials with a broad range of mechanical, chemical, and other functional properties. For instance, human finger consists of rigid bone segments connected together by using relatively flexible muscle joints and ligaments. At least two materials representing these rigid and flexible segments are required to fabricate a bioinspired finger [26, 104, 105].

In order to mimic complex natural structures, printing different materials together, known as multimaterial 3D printing, with high spatial and compositional resolution presents a great potential to the biomedical field [30, 31, 106]. However, light-based printing technologies such as SLA and pSLA are not essentially well adopted for multimaterial printing because it is difficult to dynamically switch among different resin reservoirs during printing. By contrast, FDM, DIW, and inkjet technologies can be easily utilized for multimaterial printing by incorporating multiple printheads. In particular, inkjet printing allows for voxel-by-voxel control of multiple materials composition to smoothly vary mechanical properties over different length scales [107, 108].

Bodaghi et al. [109] used Polyjet printing technology to fabricate multimaterial self-deploying mechanisms that can be used as tubular grippers for biomedical applications. In order to fabricate an active composite mechanism with programmable shape change capability, they used a multimaterial Polyjet 3D printer (Objet 500 Connex, Stratasys, Ltd) to directly print SMP fibers in an elastomeric matrix. For this purpose, two base materials, including VeroWhitePlus and TangoBlackPlus, were selected from the printer material library to print the composite actuator. VeroWhitePlus is a hard and stiff SMP, whereas TangoBlackPlus is a soft and flexible polymer. During the fabrication process, the printer is able to combine these two base materials with various ratios to get a new digital material. Three different digital materials, known as DM9850, DM9885, and DM8510 in the printer material library, with a respective T_g of 18, 31, and 64 °C, were selected to fabricate the actuator.

The actuator unit consisted of two beams; each beam had five layers with a total thickness of 1 mm. Three of these layers consisted of pure matrix (DM9850), whereas the other two were reinforced with SMP fibers (DM9885 and DM8510). Sequential thermal activation of eccentrically positioned SMP fibers with different T_g's controlled the shape change of the actuator.

Programming and actuating included these steps: The printed actuator was first heated up to 100 °C; stretched uniaxially under various nominal strains of 5%, 6.3%, 8%, and 9.25%; cooled down to 0 °C; unloaded; and finally heated up again to 90 °C. With an increase of temperature, the DM9885 SMP fibers with a low T_g of 31 °C were actuated first and applied an axial compressive force to return to their original length. The force generated by eccentrically positioned DM9885 SMP fibers produced a bending moment and resulted in an ellipsoidal shape. A further increase of temperature activated DM8510 SMP fibers with a T_g of 64 °C, which created a bending moment in reverse direction. Consequently, the actuator returned to its original straight shape at a temperature beyond the T_g's of both SMPs. Therefore, the designed actuator exhibits a two-way planar actuation.

The developed actuator unit was then used to fabricate a tubular structure with self-expanding and self-shrinking capabilities. The actuator units were arranged periodically to create a tubular shape with a length of 95 mm, a diameter of 7.7 mm, and a thickness of 1.6 mm. With an increase of temperature, the tubular actuator first expanded, then shrank, and returned back to its original shape. Self-expanding and self-shrinking capability of this actuator, resulting from the strong anisotropy introduced into the structure during the printing process, can be exploited to grip and carry an object.

14.4.2 Humidity-Actuated 4D Printing

Hydrogels are widely used to fabricate scaffolds for tissue engineering applications because they exhibit the features of a natural matrix that creates highly hydrated permeable microenvironments with tunable chemical and mechanical properties appropriate for cell culture [110–112]. They provide uniform and effective cell seeding; are able to effectively transfer physical, chemical, and biological signals; and can be formed into various 3D architectures [35].

Humidity can deform hydrogel structures through different levels of water absorption in different constituents and layers. For instance, Jamal et al. [113] used conventional photolithography to fabricate a two-layered hydrogel scaffold containing photopatterned polyethylene glycol (PEG) of different molecular weights, which exhibited self-folding capability realized by differential swelling of the two PEG bilayers. Insulin-secreting cells were encapsulated in the hydrogel scaffolds. Under humidity, the cell-laden scaffolds self-folded into cylinders. During a period of eight weeks, the scaffold exhibited a robust insulin production with a cell viability as high as 90%.

Gelation is necessary for a 3D printed hydrogel structure to maintain its shape. It is achieved through physical or chemical cross-linking or a combination of both [35]. Physical cross-linking consists of nonchemical reversible mechanisms such as entanglements of polymer chains achieved through shear-thinning property of the bioink, whereas chemical cross-linking is induced by the formation of covalent bonds. Overall, physically cross-linked hydrogels exhibit lower mechanical properties that may result in stability issues of the printed structure.

Shape-morphing architectures found in nature have many potential applications in tissue engineering and biomedical devices. One example of such structures is complex three-dimensional morphologies of plants resulting from local swelling and hydration-induced changes in their shapes caused by directional distribution of cellulose fibrils within plant cell walls. Developing an efficient one-step fabrication process to create bioinspired structures with the capability to achieve certain target shapes based on a predictive model is of great value. Gladman et al. [18] developed a plant-inspired shape-changing structure based on 4D printing. Using DIW technology, they printed a hydrophilic composite material with local control of the orientation of cellulose fibrils within a hydrogel matrix.

Hydrogel can also be used to fabricate bioinspired soft robots [114, 115]. Wehner et al. [116] used DIW technology to fabricate an entirely soft, autonomous robot inspired by octopus (Figure 14.13). The fuel reservoirs, catalytic reaction chambers, actuator networks, and vent orifices were printed from hydrogel-based inks, and the body and microfluidic logic of the robot were fabricated using soft lithography and molding. By incorporating the programmable assembly of multiple materials and parts within this structure, the developed approach allows for the design and fabrication of completely soft, autonomous robots.

Moreover, self-healing hydrogels have attracted significant attention over the past decade [117, 118]. Self-healing is one of the most remarkable features of natural tissues and organs such as skin, bones, and wood [119] and is defined as the ability of a material to self-mend damage, heal cracks, and recover its original mechanical properties so as to have a longer lifetime. Self-healing

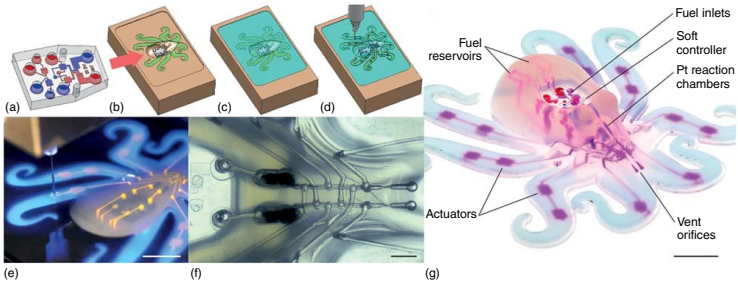

Figure 14.13 Soft robot assembly printed by DIW technology. (a–f) Fabrication steps of the assembly, including loading a prefabricated microfluidic soft controller into a mold and printing hydrogel inks. (g) The fabricate robot is removed from the mold and inverted to reveal a fully soft, autonomous robot. Source: Wehner et al. 2016 [116]. Reproduced with permission of Springer Nature.

hydrogels have the capability to heal damaged tissues and organs intrinsically and automatically, without the intervention of an external signal or stimulus, through reconstructive covalent dangling side chains or noncovalent hydrogen bonding [117]. Although there is no report of 4D printing of self-healing hydrogels in the literature, the dynamic behavior of these active materials offers a great potential for 4D printing of self-healing hydrogels for tissue and organ regeneration applications.

14.5 Conclusion and Outlook

Over the past decade, the 3D printing technologies capable of fabricating complex objects from biomaterials and cellular species have seen significant progress. However, a major drawback of the current 3D printing technologies is that they are only able to create static objects that permanently maintain their original as-printed shape. With the incorporation of various stimuli-responsive biomaterials into advanced 3D printing methodologies and integration of an additional dimension of time, 4D printing is believed to be the future technology to produce transformable objects, e.g. scaffolds used in tissue engineering, which continue to reshape after being fabricated. It is a promising technology to fabricate customized 3D biostructures with myriad applications in the biomedical field. The most common environmental stimuli used to deform 4D printed bioconstructs and medical devices include temperature, which is mostly used to actuate SMPs, and humidity, which is often used to activate hydrophilic materials.

Despite recent significant progress in the area of 4D printing, notable scientific barriers remain that prevent most transformative applications of this new technology in medicine. For further development of this new field, novel stimulus-responsive printable biomaterials with appropriate rheological behavior, identified by the viscosity, surface tension, shear yield stress, and shear elastic and loss moduli, should be optimized for rapid and effective 4D printing. The currently used SMPs used for 4D printing are "one-way," i.e. after recovering to their original as-printed shape, they cannot change their configuration any more after being cooled to a temperature lower than transition temperature, unless the loading–unloading programming step is repeated. This intrinsic irreversibility of shape memory transformation limits the application of SMPs and necessitates the incorporation of novel two-way SMPs into advanced 3D printing modalities. Alternatively, reversible shape change of bioprinted structures can be achieved by combining various types of active materials with different actuation mechanisms.

Furthermore, the current active materials used for 4D printing are only sensitive to one type of external stimulus. Active printable materials and structures that are able to respond to multiple environmental signals are highly desirable for biomedical applications because in the living organisms complicated biostructures are constantly influenced by various regulatory stimuli.

The currently used 4D printed structures show simple uniform deformations, such as twisting and bending, at the macroscale. Precise control of deformation of the 4D printed biostructures at the microscale provides new opportunities to mimic complex deformation of natural organs. To this end, developing

appropriate constitutive material models, which are able to capture time- and temperature-dependent nonlinear behavior of SAMs, is of great importance to locally control the morphology of the printed object. These models can be incorporated into computational design tools, such as finite element analysis, to predict deformation of the 4D printed objects and their stress and strain distribution under various environmental stimuli during programming and actuation and optimize the programming conditions such as deformation and temperature to achieve the desired performance.

References

1 Morrison, R.J., Hollister, S.J., Niedner, M.F. et al. (2015). Mitigation of tracheobronchomalacia with 3D-printed personalized medical devices in pediatric patients. *Science Translational Medicine* 7 (285): 285ra64.
2 Park, S.A., Lee, S.J., Lim, K.S. et al. (2015). In vivo evaluation and characterization of a bio-absorbable drug-coated stent fabricated using a 3D-printing system. *Materials Letters* 141: 355–358.
3 Bergmann, C., Lindner, M., Zhang, W. et al. (2010). 3D printing of bone substitute implants using calcium phosphate and bioactive glasses. *Journal of the European Ceramic Society* 30 (12): 2563–2567.
4 Bose, S., Vahabzadeh, S., and Bandyopadhyay, A. (2013). Bone tissue engineering using 3D printing. *Materials Today* 16 (12): 496–504.
5 Gross, B.C., Erkal, J.L., Lockwood, S.Y. et al. (2014). *Evaluation of 3D Printing and its Potential Impact on Biotechnology and the Chemical Sciences*. ACS Publications.
6 Herbert, N., Simpson, D., Spence, W.D., and Ion, W. (2005). A preliminary investigation into the development of 3-D printing of prosthetic sockets. *Journal of Rehabilitation Research and Development* 42 (2): 141.
7 Ventola, C.L. (2014). Medical applications for 3D printing: current and projected uses. *Pharmacy and Therapeutics* 39 (10): 704.
8 Rengier, F., Mehndiratta, A., von Tengg-Kobligk, H. et al. (2010). 3D printing based on imaging data: review of medical applications. *International Journal of Computer Assisted Radiology and Surgery* 5 (4): 335–341.
9 Zhang, Y.S., Yue, K., Aleman, J. et al. (2017). 3D bioprinting for tissue and organ fabrication. *Annals of Biomedical Engineering* 45 (1): 148–163.
10 Zhang, Y.S., Duchamp, M., Oklu, R. et al. (2016). Bioprinting the cancer microenvironment. *ACS Biomaterials Science and Engineering* 2 (10): 1710.
11 Murphy, S.V. and Atala, A. (2014). 3D bioprinting of tissues and organs. *Nature Biotechnology* 32 (8): 773–785.
12 Xu, F., Celli, J., Rizvi, I. et al. (2011). A three-dimensional in vitro ovarian cancer coculture model using a high-throughput cell patterning platform. *Biotechnology Journal* 6 (2): 204–212.
13 Norotte, C., Marga, F.S., Niklason, L.E., and Forgacs, G. (2009). Scaffold-free vascular tissue engineering using bioprinting. *Biomaterials* 30 (30): 5910–5917.
14 Truby, R.L. and Lewis, J.A. (2016). Printing soft matter in three dimensions. *Nature* 540 (7633): 371–378.

15 Lu, L., Mende, M., Yang, X. et al. (2012). Design and validation of a bioreactor for simulating the cardiac niche: a system incorporating cyclic stretch, electrical stimulation, and constant perfusion. *Tissue Engineering Part A* 19 (3–4): 403–414.

16 Ge, Q., Qi, H.J., and Dunn, M.L. (2013). Active materials by four-dimension printing. *Applied Physics Letters* 103 (13): 131901.

17 Tibbits, S. (2013). *The Emergence of "4D Printing"*. Long Beach, FL: TED Conference.

18 Gladman, A.S., Matsumoto, E.A., Nuzzo, R.G. et al. (2016). Biomimetic 4D printing. *Nature Materials* 15 (4): 413–418.

19 Mao, Y., Yu, K., Isakov, M.S. et al. (2015). Sequential self-folding structures by 3D printed digital shape memory polymers. *Scientific Reports* 5: 13616.

20 Raviv, D., Zhao, W., McKnelly, C. et al. (2014). Active printed materials for complex self-evolving deformations. *Scientific Reports* 4: 7422.

21 Yang, H., Leow, W.R., Wang, T. et al. (2017). 3D printed photoresponsive devices based on shape memory composites. *Advanced Materials* (33): 29, 1701627.

22 Hull, C.W. (1986). Apparatus for production of three-dimensional objects by stereolithography. Google Patents.

23 Lee, M.P., Cooper, G.J., Hinkley, T. et al. (2015). Development of a 3D printer using scanning projection stereolithography. *Scientific Reports* 5: 9875.

24 Tumbleston, J.R., Shirvanyants, D., Ermoshkin, N. et al. (2015). Continuous liquid interface production of 3D objects. *Science* 347 (6228): 1349–1352.

25 Farahani, R.D., Chizari, K., and Therriault, D. (2014). Three-dimensional printing of freeform helical microstructures: a review. *Nanoscale* 6 (18): 10470–10485.

26 Yang, Y., Chen, Y., Wei, Y., and Li, Y. (2016). Novel design and three-dimensional printing of variable stiffness robotic grippers. *Journal of Mechanisms and Robotics* 8 (6): 061010.

27 Compton, B.G. and Lewis, J.A. (2014). 3D-printing of lightweight cellular composites. *Advanced Materials* 26 (34): 5930–5935.

28 Malek, S., Raney, J.R., Lewis, J.A., and Gibson, L.J. (2017). Lightweight 3D cellular composites inspired by balsa. *Bioinspiration and Biomimetics* 12 (2): 026014.

29 Kolesky, D.B., Truby, R.L., Gladman, A. et al. (2014). 3D bioprinting of vascularized, heterogeneous cell-laden tissue constructs. *Advanced Materials* 26 (19): 3124–3130.

30 Campbell, J., McGuinness, I., Wirz, H. et al. (2015). Multimaterial and multiscale three-dimensional bioprinter. *Journal of Nanotechnology in Engineering and Medicine* 6 (2): 021005.

31 Kang, H.-W., Lee, S.J., Ko, I.K. et al. (2016). A 3D bioprinting system to produce human-scale tissue constructs with structural integrity. *Nature Biotechnology* 34 (3): 312–319.

32 Liu, W., Zhang, Y.S., Heinrich, M.A. et al. (2017). Rapid continuous multimaterial extrusion bioprinting. *Advanced Materials* (3): 29, 1604630.

33 Ding, Z., Yuan, C., Peng, X. et al. (2017). Direct 4D printing via active composite materials. *Science Advances* 3 (4): e1602890.

34 Nakamura, M., Kobayashi, A., Takagi, F. et al. (2005). Biocompatible inkjet printing technique for designed seeding of individual living cells. *Tissue Engineering* 11 (11–12): 1658–1666.

35 Malda, J., Visser, J., Melchels, F.P. et al. (2013). 25th anniversary article: engineering hydrogels for biofabrication. *Advanced Materials* 25 (36): 5011–5028.

36 Zhang, Z., Xiong, R., Corr, D.T., and Huang, Y. (2016). Study of impingement types and printing quality during laser printing of viscoelastic alginate solutions. *Langmuir* 32 (12): 3004–3014.

37 Xu, C., Zhang, M., Huang, Y. et al. (2014). Study of droplet formation process during drop-on-demand inkjetting of living cell-laden bioink. *Langmuir* 30 (30): 9130–9138.

38 Patel, D.K., Sakhaei, A.H., Layani, M. et al. (2017). Highly stretchable and UV curable elastomers for digital light processing based 3D printing. *Advanced Materials* 29 (15): 1606000.

39 Zheng, X., Deotte, J., Alonso, M.P. et al. (2012). Design and optimization of a light-emitting diode projection micro-stereolithography three-dimensional manufacturing system. *Review of Scientific Instruments* 83 (12): 125001.

40 Sun, C., Fang, N., Wu, D., and Zhang, X. (2005). Projection micro-stereolithography using digital micro-mirror dynamic mask. *Sensors and Actuators A: Physical* 121 (1): 113–120.

41 Ma, X., Qu, X., Zhu, W. et al. (2016). Deterministically patterned biomimetic human iPSC-derived hepatic model via rapid 3D bioprinting. *Proceedings of the National Academy of Sciences* 113 (8): 2206–2211.

42 Guillotin, B. and Guillemot, F. (2011). Cell patterning technologies for organotypic tissue fabrication. *Trends in Biotechnology* 29 (4): 183–190.

43 Lendlein, A. and Kelch, S. (2005). Shape-memory polymers as stimuli-sensitive implant materials. *Clinical Hemorheology and Microcirculation* 32 (2): 105–116.

44 Lendlein, A. and Kelch, S. (2002). Shape-memory polymers. *Angewandte Chemie* 41 (12): 2034–2057.

45 Long, K.N., Scott, T.F., Qi, H.J. et al. (2009). Photomechanics of light-activated polymers. *Journal of the Mechanics and Physics of Solids* 57 (7): 1103–1121.

46 Ryu, J., D'Amato, M., Cui, X. et al. (2012). Photo-origami – bending and folding polymers with light. *Applied Physics Letters* 100 (16): 161908.

47 Choi, J., Kwon, O.-C., Jo, W. et al. (2015). 4D printing technology: a review. *3D Printing and Additive Manufacturing* 2 (4): 159–167.

48 Liu, C., Qin, H., and Mather, P. (2007). Review of progress in shape-memory polymers. *Journal of Materials Chemistry* 17 (16): 1543–1558.

49 Luo, X. and Mather, P.T. (2009). Preparation and characterization of shape memory elastomeric composites. *Macromolecules* 42 (19): 7251–7253.

50 Xie, T. (2010). Tunable polymer multi-shape memory effect. *Nature* 464 (7286): 267–270.

51 Ge, Q., Luo, X., Rodriguez, E.D. et al. (2012). Thermomechanical behavior of shape memory elastomeric composites. *Journal of the Mechanics and Physics of Solids* 60 (1): 67–83.

52 Li, M.H., Keller, P., Li, B. et al. (2003). Light-driven side-on nematic elastomer actuators. *Advanced Materials* 15 (7–8): 569–572.

53 Koerner, H., Price, G., Pearce, N.A. et al. (2004). Remotely actuated polymer nanocomposites – stress-recovery of carbon-nanotube-filled thermoplastic elastomers. *Nature Materials* 3 (2): 115–120.

54 Lendlein, A., Jiang, H., Jünger, O., and Langer, R. (2005). Light-induced shape-memory polymers. *Nature* 434 (7035): 879–882.

55 Scott, T.F., Schneider, A.D., Cook, W.D., and Bowman, C.N. (2005). Photoinduced plasticity in cross-linked polymers. *Science* 308 (5728): 1615–1617.

56 Jiang, H., Kelch, S., and Lendlein, A. (2006). Polymers move in response to light. *Advanced Materials* 18 (11): 1471–1475.

57 Scott, T.F., Draughon, R.B., and Bowman, C.N. (2006). Actuation in crosslinked polymers via photoinduced stress relaxation. *Advanced Materials* 18 (16): 2128–2132.

58 Chen, S., Hu, J., Zhuo, H., and Zhu, Y. (2008). Two-way shape memory effect in polymer laminates. *Materials Letters* 62 (25): 4088–4090.

59 Chen, S., Hu, J., and Zhuo, H. (2010). Properties and mechanism of two-way shape memory polyurethane composites. *Composites Science and Technology* 70 (10): 1437–1443.

60 Huang, W., Yang, B., An, L. et al. (2005). Water-driven programmable polyurethane shape memory polymer: demonstration and mechanism. *Applied Physics Letters* 86 (11): 114105.

61 Mohr, R., Kratz, K., Weigel, T. et al. (2006). Initiation of shape-memory effect by inductive heating of magnetic nanoparticles in thermoplastic polymers. *Proceedings of the National Academy of Sciences of the United States of America* 103 (10): 3540–3545.

62 Tobushi, H., Hara, H., Yamada, E., and Hayashi, S. (1996). Thermomechanical properties in a thin film of shape memory polymer of polyurethane series. *Smart Materials and Structures* 5 (4): 483.

63 Liu, Y., Gall, K., Dunn, M.L., and McCluskey, P. (2004). Thermomechanics of shape memory polymer nanocomposites. *Mechanics of Materials* 36 (10): 929–940.

64 Liu, Y., Gall, K., Dunn, M.L. et al. (2006). Thermomechanics of shape memory polymers: uniaxial experiments and constitutive modeling. *International Journal of Plasticity* 22 (2): 279–313.

65 Yakacki, C.M., Shandas, R., Lanning, C. et al. (2007). Unconstrained recovery characterization of shape-memory polymer networks for cardiovascular applications. *Biomaterials* 28 (14): 2255–2263.

66 Wang, Z., Hansen, C., Ge, Q. et al. (2011). Programmable, pattern-memorizing polymer surface. *Advanced Materials* 23 (32): 3669–3673.

67 Qi, H.J., Nguyen, T.D., Castro, F. et al. (2008). Finite deformation thermo-mechanical behavior of thermally induced shape memory polymers. *Journal of the Mechanics and Physics of Solids* 56 (5): 1730–1751.

68 Ge, Q., Dunn, C.K., Qi, H.J., and Dunn, M.L. (2014). Active origami by 4D printing. *Smart Materials and Structures* 23 (9): 094007.

69 Wu, J., Yuan, C., Ding, Z. et al. (2016). Multi-shape active composites by 3D printing of digital shape memory polymers. *Scientific Reports* 6: 24224.

70 Yu, K., Dunn, M.L., and Qi, H.J. (2015). Digital manufacture of shape changing components. *Extreme Mechanics Letters* 4: 9–17.

71 Ge, Q., Sakhaei, A.H., Lee, H. et al. (2016). Multimaterial 4D printing with tailorable shape memory polymers. *Scientific Reports* 6: 31110.

72 Leong, T.G., Randall, C.L., Benson, B.R. et al. (2009). Tetherless thermobiochemically actuated microgrippers. *Proceedings of the National Academy of Sciences of the United States of America* 106 (3): 703–708.

73 Malachowski, K., Breger, J., Kwag, H.R. et al. (2014). Stimuli-responsive theragrippers for chemomechanical controlled release. *Angewandte Chemie* 53 (31): 8045–8049.

74 Yoon, C., Xiao, R., Park, J. et al. (2014). Functional stimuli responsive hydrogel devices by self-folding. *Smart Materials and Structures* 23 (9): 094008.

75 Lee, H., Xia, C., and Fang, N.X. (2010). First jump of microgel; actuation speed enhancement by elastic instability. *Soft Matter* 6 (18): 4342–4345.

76 Jamal, M., Zarafshar, A.M., and Gracias, D.H. (2011). Differentially photo-crosslinked polymers enable self-assembling microfluidics. *Nature Communications* 2: 527.

77 Malachowski, K., Breger, J., Kwag, H.R. et al. (2014). Stimuli-responsive theragrippers for chemomechanical controlled release. *Angewandte Chemie* 126 (31): 8183–8187.

78 Bakarich, S.E., Gorkin, R., and Spinks, G.M. (2015). 4D printing with mechanically robust, thermally actuating hydrogels. *Macromolecular Rapid Communications* 36 (12): 1211–1217.

79 Ding, Z., Weeger, O., Qi, H.J., and Dunn, M.L. (2018). 4D rods: 3D structures via programmable 1D composite rods. *Materials and Design* 137: 256–265.

80 Yuan, C., Roach, D.J., Dunn, C.K. et al. (2017). 3D printed reversible shape changing soft actuators assisted by liquid crystal elastomers. *Soft Matter* 13 (33): 5558–5568.

81 Huang, W.M., Song, C., Fu, Y.Q. et al. (2013). Shaping tissue with shape memory materials. *Advanced Drug Delivery Reviews* 65 (4): 515–535.

82 Nadgorny, M., Xiao, Z., Chen, C., and Connal, L.A. (2016). Three-dimensional printing of pH-responsive and functional polymers on an affordable desktop printer. *ACS Applied Materials and Interfaces* 8 (42): 28946–28954.

83 Gao, B., Yang, Q., Zhao, X. et al. (2016). 4D bioprinting for biomedical applications. *Trends in Biotechnology* 34 (9): 746–756.

84 Meng, H. and Li, G. (2013). A review of stimuli-responsive shape memory polymer composites. *Polymer* 54 (9): 2199–2221.

85 Hager, M.D., Bode, S., Weber, C., and Schubert, U.S. (2015). Shape memory polymers: past, present, and future developments. *Progress in Polymer Science* 49: 3–33.

86 Agrawal, D. and Habr, F.G. (2009). Removable self-expandable plastic stent to treat postphotodynamic therapy esophageal stricture. *Gastrointestinal Endoscopy* 69 (4): e27–e30.

87 Senatov, F., Niaza, K., Zadorozhnyy, M.Y. et al. (2016). Mechanical properties and shape memory effect of 3D-printed PLA-based porous scaffolds. *Journal of the Mechanical Behavior of Biomedical Materials* 57: 139–148.

88 Neuss, S., Blomenkamp, I., Stainforth, R. et al. (2009). The use of a shape-memory poly(ε-caprolactone)dimethacrylate network as a tissue engineering scaffold. *Biomaterials* 30 (9): 1697–1705.

89 Hendrikson, W.J., Rouwkema, J., Clementi, F. et al. (2017). Towards 4D printed scaffolds for tissue engineering: exploiting 3D shape memory polymers to deliver time-controlled stimulus on cultured cells. *Biofabrication* 9 (3): 031001.

90 Behl, M., Kratz, K., Zotzmann, J. et al. (2013). Reversible bidirectional shape-memory polymers. *Advanced Materials* 25 (32): 4466–4469.

91 Hearon, K., Wierzbicki, M.A., Nash, L.D. et al. (2015). A processable shape memory polymer system for biomedical applications. *Advanced Healthcare Materials* 4 (9): 1386–1398.

92 Bao, M., Lou, X., Zhou, Q. et al. (2014). Electrospun biomimetic fibrous scaffold from shape memory polymer of PDLLA-co-TMC for bone tissue engineering. *ACS Applied Materials and Interfaces* 6 (4): 2611–2621.

93 Miao, S., Zhu, W., Castro, N.J. et al. (2016). 4D printing smart biomedical scaffolds with novel soybean oil epoxidized acrylate. *Scientific Reports* 6: 27226.

94 Yang, Y., Chen, Y., Wei, Y., and Li, Y. (2016). 3D printing of shape memory polymer for functional part fabrication. *The International Journal of Advanced Manufacturing Technology* 84 (9–12): 2079–2095.

95 Tuan, H.S. and Hutmacher, D.W. (2005). Application of micro CT and computation modeling in bone tissue engineering. *Computer-Aided Design* 37 (11): 1151–1161.

96 Zarek, M., Mansour, N., Shapira, S., and Cohn, D. (2017). 4D printing of shape memory-based personalized endoluminal medical devices. *Macromolecular Rapid Communications* 38 (2): 1600628.

97 Strausz, J.B.C.T. (ed.) (2010). *Interventional Pulmonology*, 247. European Respiratory Society Journals Ltd.

98 Liu, Z., Xu, Y., Cao, L. et al. (2012). Phosphoester cross-linked vegetable oil to construct a biodegradable and biocompatible elastomer. *Soft Matter* 8 (21): 5888–5895.

99 Luo, C., Grigsby, W.J., Edmonds, N.R., and Al-Hakkak, J. (2013). Vegetable oil thermosets reinforced by tannin-lipid formulations. *Acta Biomaterialia* 9 (2): 5226–5233.

100 Garrison, T.F., Kessler, M.R., and Larock, R.C. (2014). Effects of unsaturation and different ring-opening methods on the properties of vegetable oil-based polyurethane coatings. *Polymer* 55 (4): 1004–1011.

101 Biermann, U., Bornscheuer, U., Meier, M.A. et al. (2011). Oils and fats as renewable raw materials in chemistry. *Angewandte Chemie* 50 (17): 3854–3871.

102 Liu, S.Q., Tay, R., Khan, M. et al. (2010). Synthetic hydrogels for controlled stem cell differentiation. *Soft Matter* 6 (1): 67–81.

103 Melchels, F.P., Feijen, J., and Grijpma, D.W. (2009). A poly(D,L-lactide) resin for the preparation of tissue engineering scaffolds by stereolithography. *Biomaterials* 30 (23): 3801–3809.

104 Wang, W., Rodrigue, H., Kim, H.-I. et al. (2016). Soft composite hinge actuator and application to compliant robotic gripper. *Composites Part B: Engineering* 98: 397–405.

105 Rodrigue, H., Wang, W., Kim, D.-R., and Ahn, S.-H. et al. (2017). Curved shape memory alloy-based soft actuators and application to soft gripper. *Composite Structures* 176 (15): 398–406.

106 Ober, T.J., Foresti, D., and Lewis, J.A. (2015). Active mixing of complex fluids at the microscale. *Proceedings of the National Academy of Sciences* 112 (40): 12293–12298.

107 Bartlett, N.W., Tolley, M.T., Overvelde, J.T. et al. (2015). A 3D-printed, functionally graded soft robot powered by combustion. *Science* 349 (6244): 161–165.

108 Doubrovski, E., Tsai, E.Y., Dikovsky, D. et al. (2015). Voxel-based fabrication through material property mapping: a design method for bitmap printing. *Computer-Aided Design* 60: 3–13.

109 Bodaghi, M., Damanpack, A., and Liao, W. (2016). Self-expanding/shrinking structures by 4D printing. *Smart Materials and Structures* 25 (10): 105034.

110 Nguyen, K.T. and West, J.L. (2002). Photopolymerizable hydrogels for tissue engineering applications. *Biomaterials* 23 (22): 4307–4314.

111 Drury, J.L. and Mooney, D.J. (2003). Hydrogels for tissue engineering: scaffold design variables and applications. *Biomaterials* 24 (24): 4337–4351.

112 Ifkovits, J.L. and Burdick, J.A. (2007). Photopolymerizable and degradable biomaterials for tissue engineering applications. *Tissue Engineering* 13 (10): 2369–2385.

113 Jamal, M., Kadam, S.S., Xiao, R. et al. (2013). Bio-origami hydrogel scaffolds composed of photocrosslinked PEG bilayers. *Advanced Healthcare Materials* 2 (8): 1142–1150.

114 Palleau, E., Morales, D., Dickey, M.D., and Velev, O.D. (2013). Reversible patterning and actuation of hydrogels by electrically assisted ionoprinting. *Nature Communications* 4: 2257.

115 Ionov, L. (2013). Biomimetic hydrogel-based actuating systems. *Advanced Functional Materials* 23 (36): 4555–4570.

116 Wehner, M., Truby, R.L., Fitzgerald, D.J. et al. (2016). An integrated design and fabrication strategy for entirely soft, autonomous robots. *Nature* 536 (7617): 451–455.

117 Taylor, D.L. and In Het Panhuis, M. (2016). Self-healing hydrogels. *Advanced Materials* 28 (41): 9060–9093.

118 Tuncaboylu, D.C., Sari, M., Oppermann, W., and Okay, O. (2011). Tough and self-healing hydrogels formed via hydrophobic interactions. *Macromolecules* 44 (12): 4997–5005.

119 Amendola, V. and Meneghetti, M. (2009). Self-healing at the nanoscale. *Nanoscale* 1 (1): 74–88.